

# Evidence for dust depletion in a misaligned protoplanetary disk with JWST

Espaillat, C.C.; Thanathibodee, T.; Zhu, Z.; Rabago, I.; Wendeborn, J.; Calvet, N.; ...; Yan, P.-G.

# Citation

Espaillat, C. C., Thanathibodee, T., Zhu, Z., Rabago, I., Wendeborn, J., Calvet, N., ... Yan, P. -G. (2024). Evidence for dust depletion in a misaligned protoplanetary disk with JWST. *Astrophysical Journal Letters*, *973*(1). doi:10.3847/2041-8213/ad76a5

Version: Publisher's Version

License: <u>Creative Commons CC BY 4.0 license</u>
Downloaded from: <u>https://hdl.handle.net/1887/4180134</u>

**Note:** To cite this publication please use the final published version (if applicable).

#### **OPEN ACCESS**



# Evidence for Dust Depletion in a Misaligned Protoplanetary Disk with JWST

C. C. Espaillat<sup>1,2</sup>, T. Thanathibodee<sup>1,2</sup>, Z. Zhu<sup>3,4</sup>, I. Rabago<sup>3,4</sup>, J. Wendeborn<sup>1,2</sup>, N. Calvet<sup>5</sup>, L. Zamudio-Ruvalcaba<sup>1,2</sup>, M. Volz<sup>1,2</sup>, C. Pittman<sup>1,2</sup>, M. McClure<sup>6</sup>, J. F. Babb<sup>7</sup>, R. Franco-Hernández<sup>8</sup>, E. Macías<sup>9</sup>, M. Reynolds<sup>5,10</sup>, and P.-G. Yan<sup>7</sup>, A. Reynolds<sup>5,10</sup>, and P.-G. Yan<sup>7</sup>, and

8 Instituto de Astronomía y Meteorología, Universidad de Guadalajara, Avenida Vallarta No. 2602, Col. Arcos Vallarta Sur, CP 44130, Guadalajara, Jalisco, Mexico European Southern Observatory, Karl-Schwarzschild-Str. 2, 85748, Garching bei Munchen, Germany Department of Astronomy, Ohio State University, 140 West 18th Avenue, Columbus, OH 43210, USA Received 2024 July 26; revised 2024 August 30; accepted 2024 August 30; published 2024 September 16

#### Abstract

Here we report the detection of dust depletion in a misaligned inner disk around UX Tau A using JWST MIRI spectra. Mid-infrared (MIR) continuum "seesaw" variability was detected in this disk by Spitzer and attributed to variable shadows cast on the outer disk by the inner disk. The JWST MIRI spectrum of UX Tau A also shows seesaw variability but with a significant decrease of emission shortward of  $10~\mu m$  to nearly photospheric levels. We argue that UX Tau A's MIR continuum variability is due to depletion of dust in a misaligned inner disk. We speculate that this dust depletion occurs because the inner disk is misaligned from the outer disk, which can disrupt the replenishment of the inner disk from the outer disk. Using contemporaneous measurements of the mass accretion rate of UX Tau A and estimating the amount of dust necessary to produce the MIR excess in the Spitzer observations, we estimate a minimum dust depletion timescale of  $\sim 0.1~\rm yr$ . These observations show that we can indirectly detect the signatures of misaligned inner disks through MIR continuum variability and that in some cases the inner disk may be significantly depleted of dust and become optically thin.

Unified Astronomy Thesaurus concepts: Classical T Tauri stars (252); Protoplanetary disks (1300)

#### 1. Introduction

Variability is a distinctive characteristic of low-mass ( $<2\,M_{\odot}$ ), accreting pre-main-sequence stars (i.e., Classical T Tauri stars, CTTSs). Extensive multiepoch studies of CTTSs in the X-ray, UV, optical, and IR wavelengths revealed significant variability at each of these wavelengths (e.g., J. Stauffer et al. 2015).

Out of the wide range of variability seen to date, at least two types are linked to dust in the inner regions of the protoplanetary disk: mid-infrared (MIR) "seesaw" continuum variability and optical "dipper" light curves. Seesaw variability was discovered by Spitzer, which found that the MIR continuum in many disks with large central cavity seesaws, i.e., the flux at shorter wavelengths, varies inversely with the flux at longer wavelengths (J. Muzerolle et al. 2009; C. Espaillat et al. 2011; K. M. Flaherty et al. 2011). Spectral energy distribution modeling showed that this seesawing behavior could be explained by differences in the size of the shadow cast on the edge of the outer disk by the inner disk. C. Espaillat et al. (2011) attributed the seesaw behavior to changes in the inner disk wall height resulting in differences in illumination in the outer wall, a geometrical effect. Near-infrared (NIR) imaging of dark regions supports shadowing of the outer disk by the inner disk (e.g., S. Facchini et al. 2018; Z. Zhu 2019;

Original content from this work may be used under the terms of the Creative Commons Attribution 4.0 licence. Any further distribution of this work must maintain attribution to the author(s) and the title of the work, journal citation and DOI.

R. Nealon et al. 2020; M. Benisty et al. 2023). "Dippers" were identified in Kepler surveys based on their optical light curves, which display deep dips in their brightness (A. M. Cody et al. 2014; J. Stauffer et al. 2015). The period of the dips is typically a few days and equals the stellar rotation period, which indicates that there is dust located at the corotation radius that obscures the star (J. Bouvier et al. 2007; A. M. Cody & L. A. Hillenbrand 2018).

Here, we study UX Tau A, which has been reported to display seesaw variability (C. Espaillat et al. 2011), to further explore the role of dust in the innermost disk in MIR continuum variability and the link to dippers and disk shadows. UX Tau is a quadruple system located in the Taurus-Auriga star-forming region at a distance of ~147 pc (Gaia Collaboration et al. 2018). The UX Tau system is made up of components A, B, and C where A and B are separated by 5."86 and A and C are separated by 2."63 (R. J. White & A. M. Ghez 2001). UX Tau B is a close binary separated by 0."1 (G. Duchêne et al. 2024). In this work, we focus on the A component of the UX Tau system, which has been shown to dominate the emission (R. J. White & A. M. Ghez 2001).

UX Tau A has a stellar mass of  $1.4\,M_{\odot}$  (L. A. Zapata et al. 2020) and reported spectral types of G5–K5 (A. E. Rydgren et al. 1976; P. Hartigan et al. 1989; A. L. Kraus & L. A. Hillenbrand 2009; C. Espaillat et al. 2010) with an accretion rate of  $1 \times 10^{-8}\,M_{\odot}\,\mathrm{yr}^{-1}$  (C. Espaillat et al. 2010). This object is surrounded by a pretransitional disk (i.e., an inner disk separated from an outer disk by a large gap  $\sim$  tens of astronomical units wide; C. Espaillat et al. 2014). (Sub)

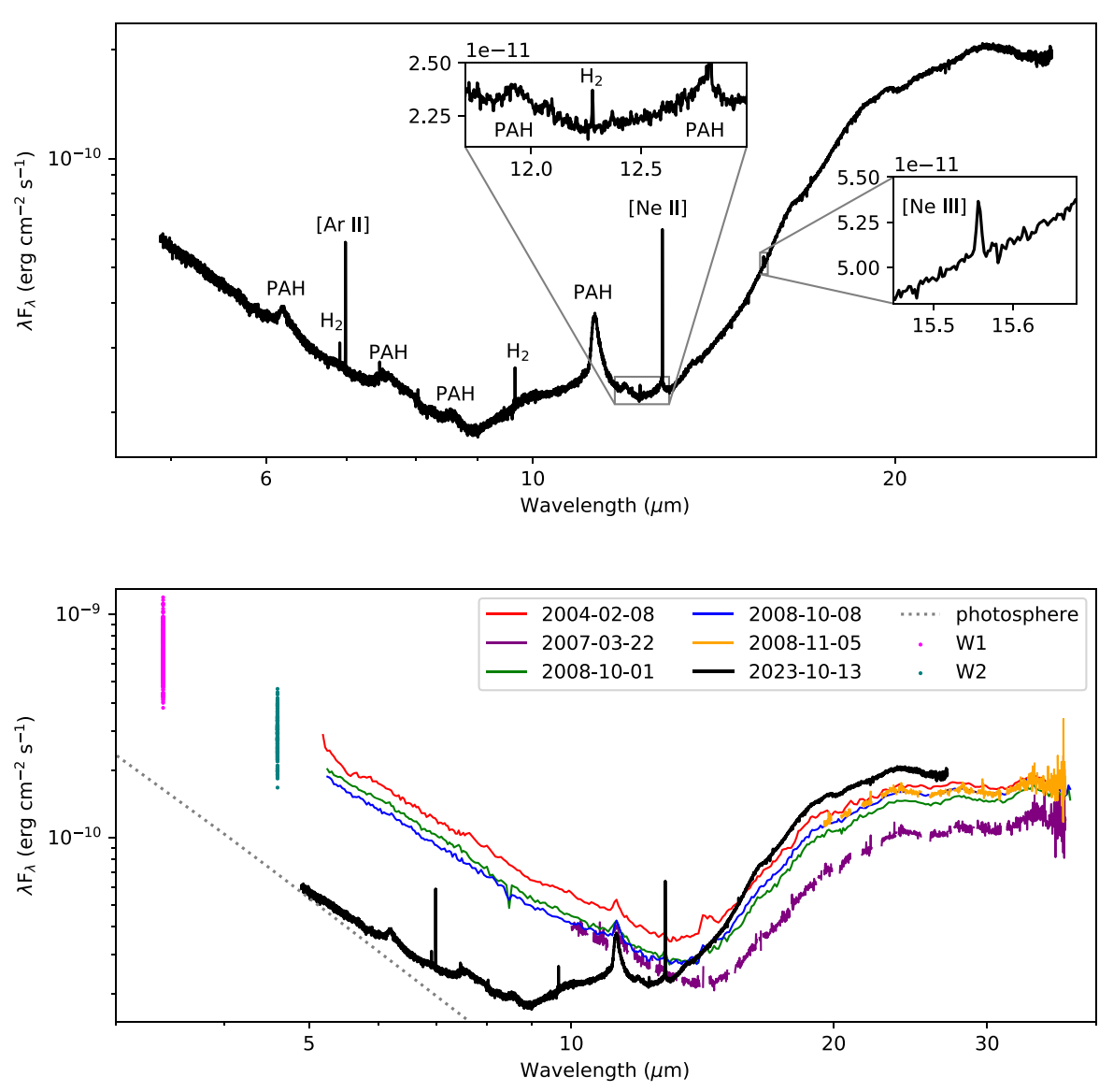


Figure 1. Top: JWST spectrum of UX Tau A with some atomic lines,  $H_2$  lines, and PAH features identified. Bottom: MIR spectra of UX Tau A displaying MIR continuum variability over  $\sim$ 19 yr (see legend). The JWST MIRI MRS spectrum is shown in black, and the other spectra are from Spitzer. We include WISE/NEOWISE W1 and W2 photometry, which are shown as magenta and teal circles. The stellar photosphere (dotted line) is adapted from C. Espaillat et al. (2011).

millimeter imaging finds that the disk has a gap of  $\sim$ 25–31 au (S. M. Andrews et al. 2011; L. Francis et al. 2020) as well as spiral arm structure indicating that UX Tau A has been perturbed by UX Tau C within the past 1000 yr (F. Ménard et al. 2020; L. A. Zapata et al. 2020). NIR observations detect dust down to at least 23 au (R. Tanii et al. 2012).

Here we present new JWST data of UX Tau A and contemporaneous optical spectra, which we compare to archival MIR spectra and photometry as well as contemporaneous optical light curves. In Section 2, we present the new and supporting data sets. In Section 3, we analyze the optical light curves and  ${\rm H}\alpha$  profiles. We discuss possible connections between the data sets in Section 4 and end with a summary in Section 5.

# 2. Observations and Data Reduction

We study MIR spectra from JWST and Spitzer, MIR photometry from Wide-field Infrared Survey Explorer (WISE)/NEOWISE, optical light curves from TESS and All-Sky

Automated Survey for Supernovae (ASAS-SN), and optical spectra from Las Cumbres Global Observatory 1 m Telescope (LCOGT)/NRES. In the following, we provide more details about these data.

# 2.1. MIR Data

# 2.1.1. JWST

We present new JWST MIRI (G. H. Rieke et al. 2015; G. S. Wright et al. 2023) Medium-resolution Spectrometer (MRS; M. Wells et al. 2015) data of UX Tau A taken on 2023 October 13 starting at 05:37:37 UT as part of General Observer (GO) program 1676 (PI: Espaillat). The observations were 336 s long and used the default four-point dither. Background observations were also taken with the same exposure time and setup. We follow the same reduction procedure as in C. C. Espaillat et al. (2023). In sum, we reduce the uncalibrated raw MRS data using the calibration reference file version jwst\_1252.pmap and the JWST Science Calibration Pipeline v.1.15.1 (H. Bushouse

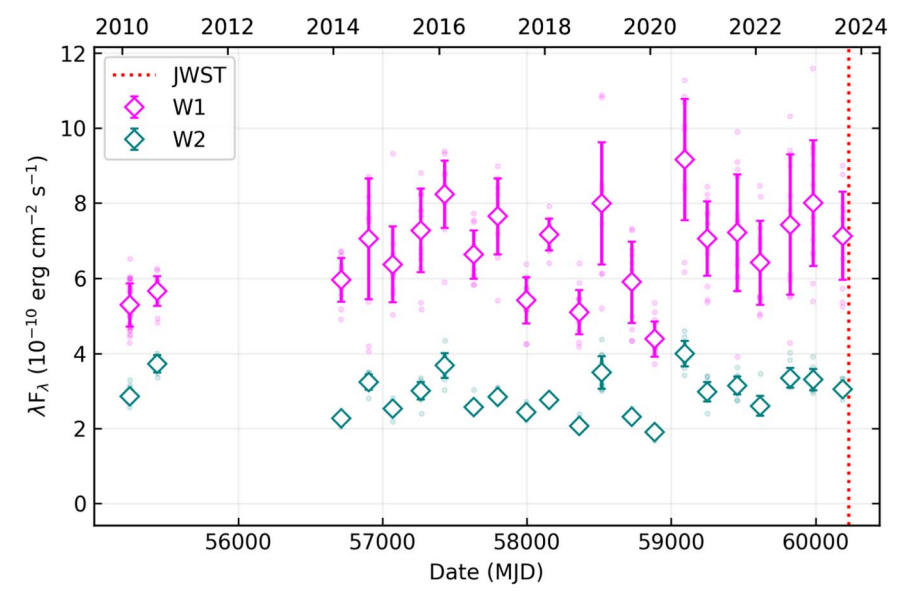


Figure 2. MIR light curve of UX Tau A from WISE/NEOWISE. The W1 and W2 data points are shown as light magenta and teal circles. The diamonds are the median flux taken over 2–3 days, and the error bars are the standard deviation. The vertical dotted line notes the time of the JWST observation.

et al. 2024). There is a known flux calibration uncertainty of  $\sim 10\%$  (D. R. Law et al. 2024, in preparation). The spectrum is presented in Figure 1.

The Channel 1 spectra (4.9–7.5  $\mu$ m) are of UX Tau A alone, while Channels 2, 3, and 4 (7.5–27.90  $\mu$ m) include the C component. At K band, the flux ratio between A and C is 16.9  $\pm$  1.6 and between A and B, it is 3.91  $\pm$  0.31 (R. J. White & A. M. Ghez 2001). If there was a significant contribution from the C component, there would have been a sharp increase in the flux at 7.5  $\mu$ m. We conclude that the C component is not contributing significantly to the MIR.

UX Tau A has detections of [Ne II] at 12.81  $\mu$ m, [Ne III] at 15.5  $\mu$ m, and [Ar II] at 6.98  $\mu$ m. There are also a few H<sub>2</sub> lines present and weak polycyclic aromatic hydrocarbons (PAH) features at  $\sim$ 6.2, 7.7, 8.6, 12.0, and 12.7  $\mu$ m along with a strong PAH feature at 11.3  $\mu$ m. We follow C. C. Espaillat et al. (2023) to measure [Ne II], [Ne III], and [Ar II] line fluxes of 1.5  $\pm$  0.1  $\times$  10<sup>-14</sup>, 1.4  $\pm$  0.3  $\times$  10<sup>-15</sup>, and 1.1  $\pm$  0.1  $\times$  10<sup>-14</sup> erg cm<sup>-2</sup> s<sup>-1</sup>. We note that the [Ne II] line flux is consistent with the line flux measured by J. Szulágyi et al. (2012).

# 2.1.2. Spitzer

In Figure 1, we show Spitzer Infrared Spectrograph (IRS) spectra taken from the Combined Atlas of Sources with Spitzer IRS Spectra (CASSIS; V. Lebouteiller et al. 2015). These include low-resolution data of UX Tau A on 2008 October 1 and 2008 October 8. Also included are high-resolution spectra of UX Tau A on 2007 March 22 and 2008 November 5. We note that the spectrum of UX Tau A from 2004 February 8 appeared to have scaling issues with the CASSIS reduction, so here we use the spectrum from C. Espaillat et al. (2011). The systematic absolute flux uncertainties on the IRS spectra are  $\sim 5\%$ .

# 2.1.3. WISE/NEOWISE

In Figure 2, we use data from from the WISE mission (E. L. Wright et al. 2010) and from the NEOWISE project (A. Mainzer et al. 2011). These data are in WISE bands W1

 $(3.4~\mu m)$  and W2  $(4.6~\mu m)$ . The WISE data are from 2010 mid-February and 2010 mid-August. The NEOWISE data span 2014 February–2023 August and are typically obtained in 2 day segments, with 10–20 observations per filter and 130–200 days between segments. The flux calibration uncertainties are less than 5%.

#### 2.2. Optical Data

#### 2.2.1. TESS and ASAS-SN

We show ASAS-SN (C. S. Kochanek et al. 2017) and TESS light curves for UX Tau A in Figure 3. The ASAS-SN *g* photometry comes from Sky Patrol V2.0 (K. Hart et al. 2023) and is contemporaneous with the JWST observations. We obtained the TESS light curves using the TESS-GAIA Light Curve (tglc) Python package (T. Han & T. D. Brandt 2023).

The TESS observations were simultaneous with JWST. TESS observed UX Tau A for  $\sim\!26$  days in Sector 70 from 2023 September 20 to October 16 (MJD: 60207.9–60233.3) with 3.3 minute cadence. In Figure 3, we include additional TESS light curves of UX Tau A from Sectors 43, 44, and 71 with cadences ranging from 3.3 to 30 minutes.

#### 2.2.2. *LCOGT*

We observed UX Tau A using the NRES spectrograph on the LCOGT. NRES is a robotic, fiber-fed spectrograph providing high-resolution ( $R \sim 48,000$ ) spectra from the BANZAI-NRES automatic reduction pipeline. Multiple exposures were stacked. All spectroscopic observations are contemporaneous with the JWST observations. UX Tau A was observed starting on 2023 October 11, 00:52 UT; 2023 October 11, 23:50 UT; 2023 October 14, 09:33 UT; and 2023 October 17, 11:20 UT. All spectra were renormalized using a polynomial fit to the continuum and are shown in Figure 4.

# 3. Analysis and Results

We measure the periods of the optical light curves and classify them following A. M. Cody et al. (2014). Then, we

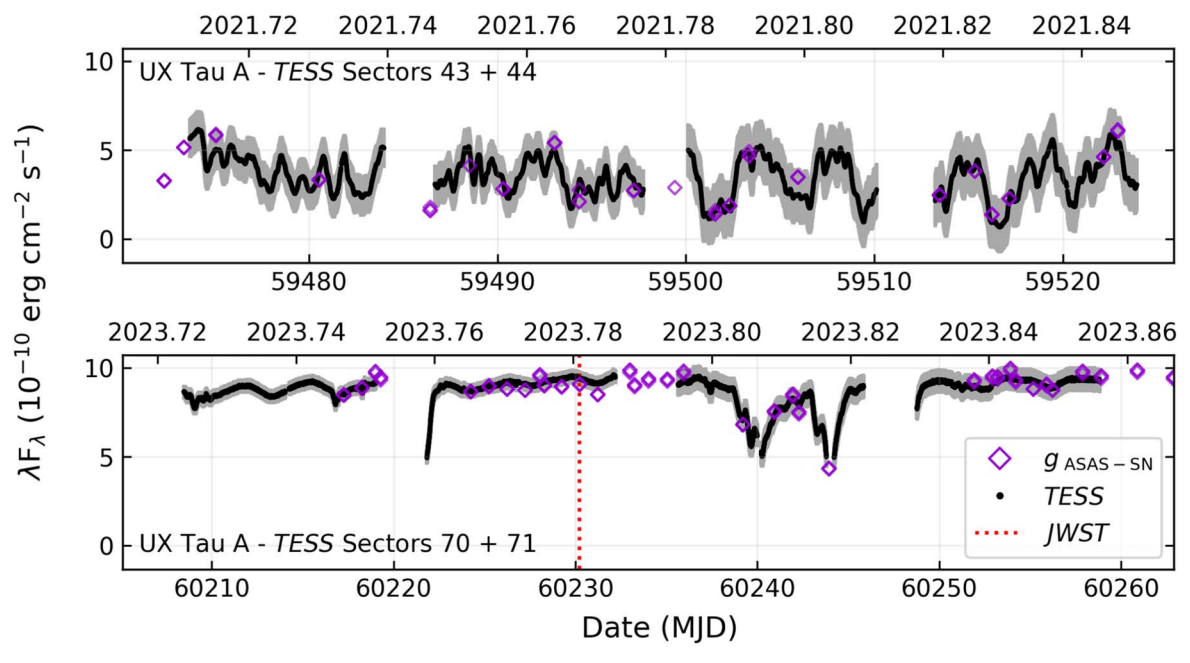


Figure 3. TESS (black line/individual black dots) and ASAS-SN *g*-band (purple) light curves of UX Tau A. To facilitate comparison, the TESS data were scaled to match the ASAS-SN data. A vertical dotted line marks the time of the JWST observation.

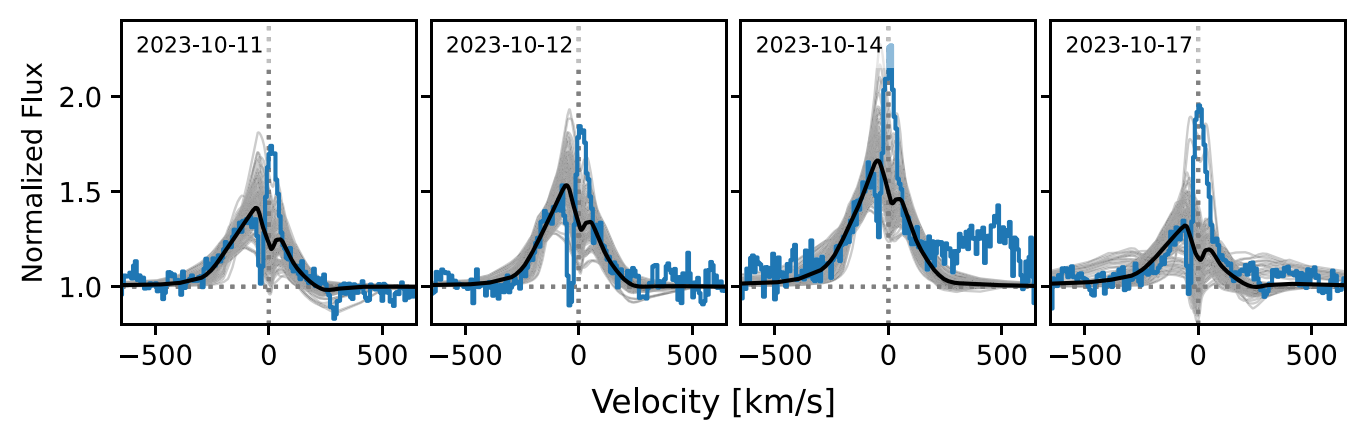


Figure 4. H $\alpha$  profiles (blue) of UX Tau A and the average accretion flow model fit (black line) along with the top 100 best-fitting models (gray lines). The horizontal and vertical dotted lines correspond to the continuum and line center, respectively.

model the  $H\alpha$  profiles to measure accretion rates and properties of the accretion flow. These results will be discussed along with the MIR data in Section 4.

# 3.1. Optical Light Curves

To measure the periods in the TESS data, we subtract a linear fit from each light curve and fit a Lomb–Scargle periodogram. We measure the Q and M variability metrics following A. M. Cody & L. A. Hillenbrand (2018). Q measures the light curve's periodicity and varies between 0 and 1, where 0 is periodic and 1 is aperiodic. Q values between 0.15 and 0.85 are quasiperiodic. M measures the light curve's asymmetry and typically varies between -1 and 1. Positive values correspond to dips and negative values to bursts, with the highest values corresponding to dippers and the lowest values to bursters. M values between  $\pm 0.25$  are symmetric.

The period of UX Tau A is  $\sim 3.8$  days among the TESS sectors (43, 44, 70, and 71). We find Q values of 0.9, 0.4, 0.9, and 0.9 and M values of -0.3, 0.2, 0.5, and 1.2. These metrics lead to the following classifications: Sector 43 burster; Sector

44 quasiperiodic symmetric (QPS); Sector 70 aperiodic dipper; and Sector 71 aperiodic dipper.

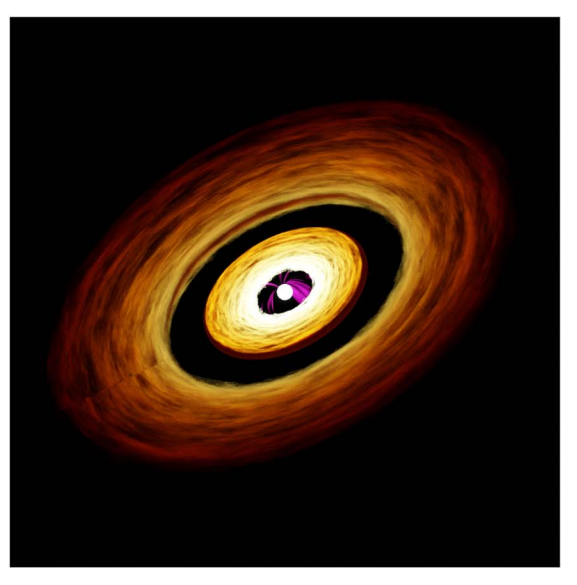
# 3.2. Optical Spectra

We model the  $\text{H}\alpha$  profiles of UX Tau A (Figure 4) using the magnetospheric accretion flow model from L. Hartmann et al. (1994) and J. Muzerolle et al. (1998, 2001). The magnetic, stellar, and disk rotation axes are aligned, and the flow geometry follows a dipolar magnetic field, which has the following parameters: inner radius ( $R_i$ ), width of the flow ( $W_r$ ) at the disk plane, maximum temperature in the flow ( $T_{\text{max}}$ ), and viewing inclination (i). To determine the best fits, we follow the procedure of T. Thanathibodee et al. (2023).

We created a grid of 29,700 models with the following values:  $\dot{M}$  (1 × 10<sup>-9</sup>-1 × 10<sup>-7</sup>  $M_{\odot}$  yr<sup>-1</sup>),  $R_{\rm i}$  (1.5-7.0  $R_{*}$ ),  $W_{\rm r}$  (0.2-1.8  $R_{*}$ ),  $T_{\rm max}$  (8-10 × 10<sup>3</sup> K), and i (20°-60°). We calculate the  $\chi^{2}$  for each combination of the model and observed profile, and we selected the models where the normalized likelihood is  $\geqslant$ 0.5 and calculated the weighted

Table 1
Results of the Magnetospheric Accretion Model

Object	Obs. Date (UT)	Instrument	$(10^{-9} \stackrel{\dot{M}}{M_{\odot}} \text{yr}^{-1})$	$R_{ m i} \ (R_{\star})$	$W_{ m r} \ (R_{\star})$	$T_{\text{max}}$ $(10^3 \text{ K})$	i (deg)
UX Tau A	2023-10-11	NRES	$16.0 \pm 29.2$	$2.3 \pm 1.6$	$0.4 \pm 0.3$	$9.0 \pm 0.7$	$46 \pm 14$
UX Tau A	2023-10-12	NRES	$11.7 \pm 22.0$	$2.0 \pm 1.2$	$0.4 \pm 0.3$	$9.0 \pm 0.6$	$46 \pm 13$
UX Tau A	2023-10-14	NRES	$21.6 \pm 31.7$	$1.7 \pm 0.4$	$0.3 \pm 0.2$	$9.0 \pm 0.6$	$48 \pm 12$
UX Tau A	2023-10-17	NRES	$11.3\pm26.9$	$3.5\pm2.2$	$0.7 \pm 0.6$	$8.7 \pm 0.7$	$36 \pm 16$



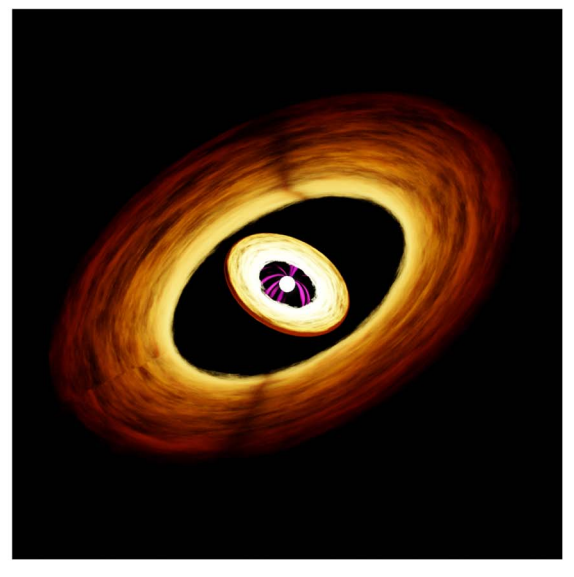


Figure 5. Schematics showing that the inner and outer disks are coplanar (left) and misaligned (right). If the inner disk has nodal precession along the vertical direction, it changes from the left to right panel after half the precession cycle.

mean of  $\dot{M}$ ,  $R_{\rm i}$ ,  $W_{\rm r}$ ,  $T_{\rm max}$ , and i. The best-fit parameters are listed in Table 1.

# 4. Discussion

Seesaw variability is still present in the JWST spectrum of UX Tau A but differs significantly from what has been seen previously. Strikingly, the JWST spectrum is nearly consistent with photospheric emission at the shortest wavelengths, with a very small MIR excess shortward of 10  $\mu m$  and a broad, weak 10  $\mu m$  silicate emission feature. This combination points to a small amount of  $\sim$ micron-sized dust grains in an optically thin inner disk. Previous work has reproduced the 10  $\mu m$  feature of UX Tau A using a grain size distribution of  $a^{-3.5}$ , where a varies between  $a_{\rm min}=0.005~\mu m$  and  $a_{\rm max}=10~\mu m$  (C. Espaillat et al. 2011).

We propose that the drop to nearly photospheric levels in UX Tau A is due to dust depletion in a misaligned inner disk undergoing disk breaking. Disk breaking is a phenomenon that occurs when the inner and outer disks precess independently, possibly due to the presence of a companion (Z. Zhu 2019). The inclination of the outer disk of UX Tau A is  $37.96^{+0.97}_{-0.90}$ , while the inclination of the inner disk is  $73.46^{+11.76}_{-16.47}$  (A. J. Bohn et al. 2022).

As the inner disk precesses, there will be times when it is aligned with the outer disk (Figure 5, left) and times when it is misaligned (Figure 5, right). Mass transfer from the outer disk to the inner disk is easiest when the disks are coplanar and is the most disrupted when the inner disk is at maximum misalignment from the outer disk. However, accretion may still occur at intermediate points. Because it only takes a small amount of dust to make the disk optically thick, any accretion can deposit sufficient dust to lead to an optically thick inner disk. Therefore, we expect that a significant MIR excess would be seen most of the time. Then, when the accretion to the inner disk is significantly disrupted, most of the dust in the inner disk may accrete or drift to the star due to lack of replenishment from the outer disk. The inner disk becomes optically thin, and there will be a drop at the shorter wavelengths in the JWST spectrum, while there is an increase at the longer wavelengths as there is little/no shadow cast on the outer disk. Below, we estimate the dust depletion and precession timescales and consider this proposed scenario in light of the MIR light curve, optical light curves, and the MIR emission lines and features.

# 4.1. Depletion and Precession Timescales

We can estimate the dust depletion timescale by calculating how much mass was in the inner disk at the time of the Spitzer observations and comparing this to the accretion rate of UX Tau A. Assuming the excess MIR emission comes from a marginally optically thick inner disk at 1550 K, the lower limit of the dust mass in the inner disk is then  $\sim\!10^{-11}\,M_{\odot}$ , using a dust opacity of  $200\,\mathrm{cm}^2\,\mathrm{g}^{-1}$  (T. Birnstiel et al. 2018). We measure accretion rates of  $1\text{--}2\times10^{-8}\,M_{\odot}\,\mathrm{yr}^{-1}$ 

 $<sup>\</sup>overline{11}$  The photosphere plotted in Figure 1 uses colors from S. J. Kenyon & L. Hartmann (1995), is scaled at J band, and follows a Rayleigh–Jeans tail beyond K band. The photometry used in C. Espaillat et al. (2011) included emission from the A, B, and C components, and here we scale the photosphere following the flux ratios from R. J. White & A. M. Ghez (2001) to represent the emission from only the A component.

contemporaneous with the JWST observations (Table 1), which would quickly deplete the inner disk of dust in 0.1 yr. Here we adopt the typically assumed dust-to-gas ratio of 0.01, but the dust-to-gas ratio in circumstellar disks is unknown, and it is not clear what it would be in the inner disk of UX Tau A.

We can also consider the precession timescale of the inner disk of UX Tau A. Theoretical works show that a misaligned Jupiter-mass planet can drive misalignment and precession of the inner disk at  $\sim 1000$  times the planetary orbital timescale (e.g., Z. Zhu 2019). We assume that the period measured from the TESS light curves (Figure 3) is the stellar rotation period. Then, if a misaligned Jupiter-mass planet is around the corotation radius, the inner disk's precession timescale is  $\sim 500$  weeks or 10 yr. If the planet is 10 Jupiter masses, the precession timescale is then 1 yr.

# 4.2. MIR Light Curve

There are no significant dips in the WISE/NEOWISE fluxes. Our estimated dust depletion timescale is  $\sim$ 0.1 yr ( $\sim$ 37 days), and the dust replenishment timescale would be similar. Since there are at least 130 days in between the segments of the WISE/NEOWISE data, it is possible that we missed this shortlived depleted period. If the precession timescale is 10 yr, the last time that the inner disk was in the same position as in the JWST observation would have been in 2013, which falls in the  $\sim$ 3.5 yr gap in coverage between WISE and NEOWISE. It is plausible that, given the sparse time cadence of the data and the short depletion and replenishment timescale, another significant MIR dip was not observed.

There is significant MIR emission in the last NEOWISE observation taken  $\sim\!43$  days before the JWST observations, which implies a quick drop to nearly photospheric levels. This is still consistent with our estimated depletion timescale. During the last NEOWISE observations, the inner disk could have been marginally optically thick, and then it became optically thin when observed with JWST. However, the estimated depletion timescale is a lower limit, and any slightly longer timescale would not be consistent with the observations.

# 4.3. Optical Light Curves

One may speculate that the drop in the JWST spectrum is due to an edge-on inner disk. However, we can exclude the possibility that the inner disk of UX Tau A was close to edge-on at the time of the JWST observations since there is no evidence of extinction of the star by the inner disk in the simultaneous optical light curve (Figure 3).

The dips in the TESS light curve suggest that there is dust in the inner disk along our line of sight, which obscures the star a few days before and after the JWST observations. This is consistent with the JWST spectrum whose small MIR excess shows that there is still some small amount of dust grains in the inner disk dust. The exact mechanism by which this dust obscures the star in the UX Tau A system is unclear. Scenarios that have been proposed to explain dippers include dusty accretion flows (E. Nagel et al. 2024), disk warps (P. T. McGinnis et al. 2015), and dusty disk winds (E. Gaidos et al. 2024).

Finally, we see a change in UX Tau A's optical light-curve behavior that could possibly be further evidence of a precessing misaligned inner disk. In 2021 (top, Figure 3), UX Tau A had a QPS light curve and 2 yr later (bottom, Figure 3) showed a

dipper light curve. This could indicate that the inner disk was at different inclinations in 2021 and 2023, changing the obscuration of the star and leading to the different light-curve behavior. This may have implications on a subset of objects with "hybrid" optical light curves, which switch from quasiperiodic to dipper (P. T. McGinnis et al. 2015; A. M. Cody & L. A. Hillenbrand 2018).

#### 4.4. MIR Atomic Gas Emission Lines and PAH Features

The proposed scenario of a depleted inner disk also appears roughly consistent with the lines and features seen in the JWST spectrum. First, only the 11.3  $\mu$ m PAH feature was clearly seen in the Spitzer spectrum (D. M. Watson et al. 2009), whereas they are all prominent in the JWST spectrum. The PAH features were likely "drowned out" in the Spitzer spectrum due to the significant MIR excess. In the JWST spectrum, the depletion of dust from the inner disk leads to a decrease in the continuum emission, allowing the PAHs to be conspicuous. Likewise, it is easier to see the [Ar II] and [Ne II] emission lines due to the decreased MIR continuum, as has been seen in other pretransitional and transitional disks (C. Espaillat et al. 2007, 2013). In addition, the presence of the [Ar II] and [Ne II] lines confirms that there is gas in the inner disk, consistent with the measured accretion rates in this work, which points to a significant gas reservoir in the inner disk despite the depletion of dust.

# 5. Summary and Conclusions

We presented a new JWST spectrum of UX Tau A, which shows a striking decrease of continuum emission shortward of  $10\,\mu\text{m}$ , dropping to nearly photospheric levels. We conclude that the dust in the inner disk has been depleted to the point where the inner disk is optically thin, leading to this drop in MIR emission. This dust depletion could be due to a disruption in the replenishment of the inner disk since accretion from the outer disk may be more difficult when the inner and outer disks are misaligned.

Monitoring of the precession timescale via inclination measurements, MIR spectra, and/or imaging is necessary to test if this variability is periodic, which would be expected if it is due to disk precession. More detailed modeling with nonaxisymmetric disks is also necessary. These approaches will help us link the variability seen in protoplanetary disks at different wavelengths.

# Acknowledgments

We acknowledge support from JWST grant GO-01676. We thank the anonymous referee for a constructive report, which improved the Letter.

The JWST data presented in this Letter were obtained from the Mikulski Archive for Space Telescopes (MAST) at the Space Telescope Science Institute. The specific observations analyzed can be accessed via doi:10.17909/sej8-g173.

Facilities: ASAS-SN, JWST, LCOGT, WISE, NEO-WISE, TESS.

# **ORCID iDs**

C. C. Espaillat https://orcid.org/0000-0001-9227-5949
T. Thanathibodee https://orcid.org/0000-0003-4507-1710

Z. Zhu https://orcid.org/0000-0003-3616-6822

I. Rabago https://orcid.org/0000-0001-5008-2794
J. Wendeborn https://orcid.org/0000-0002-6808-4066
N. Calvet https://orcid.org/0000-0002-3950-5386
L. Zamudio-Ruvalcaba https://orcid.org/0000-0001-9219-7696
M. Volz https://orcid.org/0009-0005-4517-4463
C. Pittman https://orcid.org/0000-0001-9301-6252
M. McClure https://orcid.org/0000-0003-1878-327X
J. F. Babb https://orcid.org/0000-0002-3883-9501
R. Franco-Hernández https://orcid.org/0000-0002-1650-3740
E. Macías https://orcid.org/0000-0003-1283-6262

M. Reynolds https://orcid.org/0000-0003-1621-9392

P.-G. Yan https://orcid.org/0000-0003-1623-1391

- References
- Andrews, S. M., Wilner, D. J., Espaillat, C., et al. 2011, ApJ, 732, 42 Benisty, M., Dominik, C., Follette, K., et al. 2023, in ASP Conf. Ser. 534, Protostars and Planets VII, ed. S. Inutsuka et al. (San Francisco, CA: Birnstiel, T., Dullemond, C. P., Zhu, Z., et al. 2018, ApJL, 869, L45 Bohn, A. J., Benisty, M., Perraut, K., et al. 2022, A&A, 658, A183 Bouvier, J., Alencar, S. H. P., Boutelier, T., et al. 2007, A&A, 463, 1017 Bushouse, H., Eisenhamer, J., Dencheva, N., et al. 2024, JWST Calibration Pipeline, v1.15.1, Zenodo, doi:10.5281/zenodo.6984365 Cody, A. M., & Hillenbrand, L. A. 2018, AJ, 156, 71 Cody, A. M., Stauffer, J., Baglin, A., et al. 2014, AJ, 147, 82 Duchêne, G., LeBouquin, J.-B., Ménard, F., et al. 2024, A&A, 686, A188 Espaillat, C., Calvet, N., D'Alessio, P., et al. 2007, ApJL, 664, L111 Espaillat, C., D'Alessio, P., Hernández, J., et al. 2010, ApJ, 717, 441 Espaillat, C., Furlan, E., D'Alessio, P., et al. 2011, ApJ, 728, 49 Espaillat, C., Ingleby, L., Furlan, E., et al. 2013, ApJ, 762, 62 Espaillat, C., Muzerolle, J., Najita, J., et al. 2014, in Protostars and Planets VI, ed. H. Beuther et al. (Tucson, AZ: Univ. of Arizona Press), 497 Espaillat, C. C., Thanathibodee, T., Pittman, C. V., et al. 2023, ApJL, 958, L4

```
Facchini, S., Juhasz, A., & Lodato, G. 2018, MNRAS, 473, 4459
Flaherty, K. M., Muzerolle, J., Rieke, G., et al. 2011, ApJ, 732, 83
Francis, L., Johnstone, D., Herczeg, G., Hunter, T. R., & Harsono, D. 2020, AJ,
Gaia Collaboration, Brown, A. G. A., Vallenari, A., et al. 2018, A&A, 616, A1
Gaidos, E., Thanathibodee, T., Hoffman, A., et al. 2024, ApJ, 966, 167
Han, T., & Brandt, T. D. 2023, AJ, 165, 71
Hart, K., Shappee, B. J., Hey, D., et al. 2023, arXiv:2304.03791
Hartigan, P., Hartmann, L., Kenyon, S., Hewett, R., & Stauffer, J. 1989, ApJS,
  70, 899
Hartmann, L., Hewett, R., & Calvet, N. 1994, ApJ, 426, 669
Kenyon, S. J., & Hartmann, L. 1995, ApJS, 101, 117
Kochanek, C. S., Shappee, B. J., Stanek, K. Z., et al. 2017, PASP, 129, 104502
Kraus, A. L., & Hillenbrand, L. A. 2009, ApJ, 704, 531
Lebouteiller, V., Barry, D. J., Goes, C., et al. 2015, ApJS, 218, 21
Mainzer, A., Bauer, J., Grav, T., et al. 2011, ApJ, 731, 53
McGinnis, P. T., Alencar, S. H. P., Guimarães, M. M., et al. 2015, A&A,
Ménard, F., Cuello, N., Ginski, C., et al. 2020, A&A, 639, L1
Muzerolle, J., Calvet, N., & Hartmann, L. 1998, ApJ, 492, 743
Muzerolle, J., Calvet, N., & Hartmann, L. 2001, ApJ, 550, 944
Muzerolle, J., Flaherty, K., Balog, Z., et al. 2009, ApJL, 704, L15
Nagel, E., Bouvier, J., & Duarte, A. E. 2024, A&A, 688, A61
Nealon, R., Price, D. J., & Pinte, C. 2020, MNRAS, 493, L143
Rieke, G. H., Wright, G. S., Böker, T., et al. 2015, PASP, 127, 584
Rydgren, A. E., Strom, S. E., & Strom, K. M. 1976, ApJS, 30, 307
Stauffer, J., Cody, A. M., McGinnis, P., et al. 2015, AJ, 149, 130
Szulágyi, J., Pascucci, I., Ábrahám, P., et al. 2012, ApJ, 759, 47
Tanii, R., Itoh, Y., Kudo, T., et al. 2012, PASJ, 64, 124
Thanathibodee, T., Molina, B., Serna, J., et al. 2023, ApJ, 944, 90
Watson, D. M., Leisenring, J. M., Furlan, E., et al. 2009, ApJS, 180, 84
Wells, M., Pel, J. W., Glasse, A., et al. 2015, PASP, 127, 646
White, R. J., & Ghez, A. M. 2001, ApJ, 556, 265
Wright, E. L., Eisenhardt, P. R. M., Mainzer, A. K., et al. 2010, AJ, 140, 1868
Wright, G. S., Rieke, G. H., Glasse, A., et al. 2023, PASP, 135, 048003
Zapata, L. A., Rodríguez, L. F., Fernández-López, M., et al. 2020, ApJ,
  896, 132
Zhu, Z. 2019, MNRAS, 483, 4221
```